Desalination and Water Treatment
www.deswater.com

doi:10.5004/dwt.2018.22591

120 (2018) 1–8
July

Key factors affecting water permeate velocity in reverse osmosis based on concentration polarization model

Ibrahim S. Al-Mutaz*, Fahed M. Alsubaie, Irfan Wazeer

Chemical Engineering Dept., College of Engineering, King Saud University, P O Box 800, Riyadh 11421, Saudi Arabia, email: almutaz@ksu.edu.sa (I.S. Al-Mutaz)

Received 15 January 2018; Accepted 5 June 2018

ABSTRACT

The accumulation of salts on the high-pressure side of the reverse osmosis membrane surface is attributed to concentration polarization. The efficiency of the reverse osmosis process is significantly affected due to concentration polarization. Because the value of salt concentration exceeds the bulk salt concentration at the membrane surface resulting in a salt boundary layer at the surface of the membrane. In this research, a parametric analysis was performed using the developed concentration polarization model to present qualitative and quantitative evaluations of the influence of different parameters on the overall process performance concerning membrane permeate flux. The objective of this sub-task is to illustrate the effects of physical and operating parameters on permeate velocity, wall concentration, concentration polarization factor and boundary layer thickness.

Keywords: Membrane processes; Reverse osmosis; Permeate flux; Concentration polarization

1. Introduction

Water scarcity is becoming a growing issue worldwide due to increasing population and deteriorating of supplies of water useable for irrigation, drinking and industry [1,2]. Desalination is one of the solutions for dealing with water shortages problems [3,4]. Presently, many countries including Gulf Cooperation Council countries (GCC) are using desalination methods to produce industrial and potable water for their requirements [5]. Reverse osmosis (RO) and thermal desalination processes such as multi-effect desalination (MED) and multi-stage flash (MSF) are the most commonly used desalination techniques. Over the last few years, RO is rapidly gaining market share due to significant improvements in membrane technologies used for water desalination to enhance the efficiency and cost-effectiveness of the processes [6–10]. RO is a pressure-driven separation process in which diffusion of salts and water takes place through a dense membrane. As compared to water, the diffusion of salts is much lower resulting in a rejection of the salts. This phenomenon causes rejected salts to accumulate on the membrane surface. So, the rejected matter accumulates in front of the membrane, with the highest concentration directly at the surface of the membrane. One of the most vital factors affecting the performance of membrane separation processes is concentration polarization (CP) [11]. Prediction of factors affecting water permeate velocity is crucial for designing RO processes.

The efficiency of RO plants is quite subtle to the operating conditions of plant and the feed water quality. Therefore, it is important to have efficient RO models for process operation and design [12]. However, it is not easy to achieve a stringent mechanistic model of RO plant, which considers several important parameters such as water permeate velocity, flux, concentration polarization, feed temperature and fouling. Various tools and software have been developed by the researchers to design an RO plant, nevertheless, these models mainly focus on the system performance of RO processes rather than the optimization of RO modules regarding product water quality and energy efficiency [13].

Kim and Hoek compared the available analytical CP models to a more rigorous numerical model and experimental CP data [11]. They developed a two-dimensional numerical CP model to enable the local description of sol-

*Corresponding author.

1944-3994 / 1944-3986 © 2018 Desalination Publications. All rights reserved.

ute rejection and permeate flux in crossflow reverse osmosis membrane separations. They compared the predictions of the numerical data and two analytical CP models to experimental RO performance data. The numerical and film theory models predicted channel-averaged experimental salt rejection data and experimental permeate flux accurately at operating conditions.

Oh et al. used a simple model based on the solution-diffusion theory and multiple fouling mechanisms to investigate the performance of RO systems for water desalination [13]. They analyzed the effect of permeate flux and recovery ratio on the efficiency of the RO process for different operating conditions. They used their model for the optimization of RO system for high boron removal and low energy consumption. The model can be used to determine the optimum recovery and flux for a given condition of boron concentration in permeate and specific energy.

Sempere and co-authors used Digital Holographic Interferometry (DHI) to visualize the polarization concentration layer during crossflow RO [14]. They performed the experiments with NaCl and Na_2SO_4 solutions and studied the influence of initial concentration, the pressure applied and crossflow (CF) velocity. The CF velocity was changed every 30 min in each experiment, and the steady-state was reached within few minutes after changing the CF velocity. A close relationship was found between CF velocities, polarization layer and permeate flux. Furthermore, they also reported that the permeate flux increased at higher values of CF velocities because of greater shear force occurred with the increase of the fluid flow. Radu et al. developed a two-dimensional mathematical model to investigate the effect of CF velocity in RO/nanofiltration (NF) feed channels [15]. They evaluated biofilm removal approaches based on velocity variations. Due to substrate CP, the overall substrate consumption rate dominated over accumulation with an increased biofilm thickness. Consequently, substrate concentrations decreased in the biofilm compared to bulk liquid.

Zhou et al. developed a macroscopic method to evaluate the effect of CP on the efficiency of the spiral wound membrane modules [16]. A mathematical model was proposed with the introduction of a polarization factor for the permeate flux in the spiral wound modules. The developed model was solved numerically to analyze the performance of a long membrane network under different operation parameters. They stated that the proposed model provide a feasible way to estimate CP in spiral wound modules. They also mentioned that the polarization factor increases with increasing permeate velocity. Subramani and Hoek used direct microscopic observation to investigate the physicochemical factors causing initial rates of microbial deposition onto RO and NF membrane [17]. They reported that the deposition rates increased with decreasing CF velocity, increasing salt rejection, increasing cell size, increasing membrane surface area and increasing permeate velocity. Fletcher and Wiley studied the effect of different operating conditions and geometrical parameters on the behavior of membrane systems [18]. They also investigated the influence of gravity on the variation of the permeate velocity across the membrane and reported that the gravity has a significant influence throughout the membrane channel.

In the previous work [19], an explicit expression for the water permeate velocity through the reverse osmosis process was developed by combining the solution diffusion transport model and film theory, so called concentration polarization (CP) model. This CP model assists in the formulation of concentration polarization using limited data on water, salt and membrane properties as well as the mass transfer coefficients. In this work, a parametric analysis was performed using the developed CP model to study the influence of various parameters on the performance of membrane concerning membrane permeate flux. The influence of operating and physical parameters on wall concentration, concentration polarization factor, permeate velocity and boundary layer thickness will be explored in this study.

2. Estimation of water permeate velocity

The following relation can be used to calculate the local permeate velocity, $V(x)$ which was derived and explained in detail in our previous work [19]. Fig. 1 shows the schematic of the boundary layer adjacent to the membrane surface.

$$V(x)=\sqrt[3]{\left[\left(\Delta F^3\frac{\sqrt{\frac{24\Delta F^2x+5Ns^3}{\left(6\Delta F^2x+Ns^3\right)}}}{6\Delta F^2x+Ns^3}\right)+\frac{2\Delta F^3}{6\Delta F^2x+Ns^3}\right]}-\left[\Delta F\frac{Ns}{6\Delta F^2x+Ns^3\sqrt[3]{\left[\left(\frac{\sqrt{\frac{24\Delta F^2x+5Ns^3}{\left(6\Delta F^2x+Ns^3\right)}}}{6\Delta F^2x+Ns^3}\right)+\frac{2\Delta F^3}{6\Delta F^2x+Ns^3}\right]}}\right] \quad (1)$$

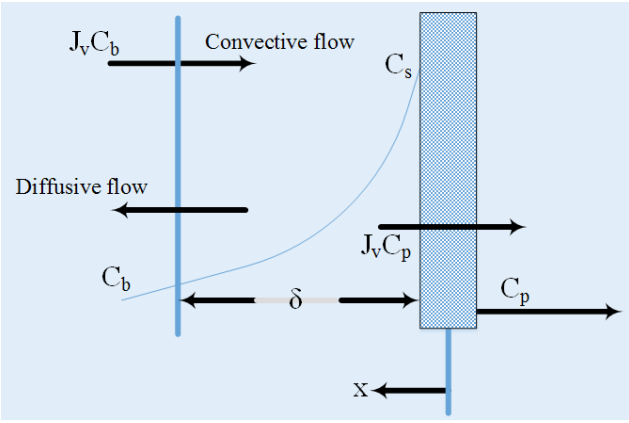

Fig. 1. Layout of the boundary layer adjacent to the surface of membrane.

The developed equation for the local permeate velocity, Eq. (1), contains two dimensionless parameters (ΔF and N_s) that need to be determined in order to predict permeate velocity using the model.

$$\Delta F = \frac{\Delta P - \Delta\pi}{\Delta\pi} \tag{2}$$

$$N_s = R_m\left(\frac{1}{\Delta\pi}\right)\left(\frac{D^2\gamma}{L}\right)^{1/3} \tag{3}$$

where Δp is the applied pressure, $\Delta\pi$ is the osmotic pressure, R_m is the membrane resistance, D is the diffusion coefficient, L is channel length and γ is the wall shear rate. ΔF and N_s are the dimensionless driving force and dimensionless membrane resistance, respectively [19]. The dimensionless parameters were introduced during the derivation of the water permeation velocity for simplifying the complex mathematical form as described in the previous work [19]. These parameters depend on solution properties and system parameters as well as the mass transfer coefficient. The mass transfer coefficient can be estimated from the correlation between Sherwood, Reynolds and Schmidt numbers as follows [20]:

$$Sh = \frac{K_b d}{D_s} = \lambda\cdot \mathrm{Re}^a\cdot S_{ci}^b\cdot\left(\frac{d_h}{W}\right)^c,\ \mathrm{Re} = \frac{du\rho}{\mu}, S_{ci} = \frac{\mu}{\rho D_s}$$

where d is the height of feed channel, u is the cross flow velocity, μ and ρ are the viscosity and density of water, respectively. The constants λ, a, b and c are mass transfer coefficient constants and their values are $\lambda = 0.065$, a = 0.875, b = 0.25 and c = 0.00 [20].

3. Results and discussion

The obtained equation for water permeate velocity is used to study the effect of various operating parameters. The permeate water velocity is given by Eq. (1) and the wall concentration is given by [11]:

$$C_w(x) = \frac{\Delta p - \frac{V_x}{A} + \phi(1-R_0)C_b}{\phi} \tag{4}$$

where $C_w(x)$ is the wall concentration, A is the membrane water permeability, ϕ is the osmotic pressure coefficient, R_o is the membrane salt rejection and C_b is the bulk concentration. To study the effect of operating parameters on mass transfer coefficient, Eq. (5) can be used, which is known as concentration polarization factor [19]. Table 1 shows the input data for the results of the obtained model.

$$\frac{C_w - C_p}{C_b - C_p} = e^{\frac{J_v}{K_b}} \tag{5}$$

where $K_b = \frac{D_s}{\delta}$ is defined as mass transfer coefficient, m/s.

3.1. Effect of operating parameters on product flux

The most important operating parameters that affect the product flux are applied pressure, feed concentration and membrane water permeability. In this section, the effect of these parameters was discussed in detail. Table 2 shows the values of permeate velocity ($V(x)$), wall concentration, concentration polarization factor and boundary layer thickness against the applied pressure. The effect of applied pressure on water permeate velocity is depicted in Fig. 2. It is clear from the figure that permeate velocity increases as applied pressure increases. This is supported by the basic reverse osmosis equation [Eq.(6)] [19]. An increase in applied pressure by 17% yield an increase of 8% in permeate velocity as can be seen in Fig. 2. A large driving force for permeation is induced due to higher applied pressure. In addition, the permeate velocity showed almost linear dependence on the applied pressure.

$$Q_w = A(\Delta P - \Delta\pi) \tag{6}$$

where Q_w is the rate of water flow through the membrane, ΔP is the hydraulic pressure differential across the membrane, $\Delta\pi$ is the osmotic pressure differential across the membrane, A is the membrane permeability coefficient for water.

Table 1
General values of operating parameters

Parameter	Value
Applied pressure Δp, Pa	2×10^6
Osmotic pressure coefficient ϕ, Pa/mol	4955.1
Membrane water permeability A, m·pa^{-1} s^{-1}	2×10^{-11}
Wall shear rate, s^{-1}	1000
Membrane salt rejection R_o	1
Channel length L, m	1
Viscosity of water μ, N·s/m^{-2}	1.0×10^{-3}
Water cross flow velocity u, m/s	0.1
Hydraulic diameter of channel d, m	1.4×10^{-3}
Density of water ρ, kg/m^3	1000
Diffusion coefficient D, m^2/s	1.6×10^{-9}
Membrane resistance R_m, pa·s/m	1.0×10^{11}
Bulk concentration C_b, mol/m^3	85.5
Reynolds number R_e	140
Schmidt number S_c	625
Sherwood number S_h	24.53
Mass transfer coefficient K_b, m/s	2.8×10^{-5}

Table 2
Effect of applied pressure, Δp on water permeate velocity, wall concentration, concentration polarization factor and boundary layer thickness

Δp, pa	$V_{(x)}$, m/s	C_w, mol/m^3	C_w/C_b	δ, m	D_s/δ
1×10^6	3.96×10^{-6}	162.0	1.890	2.57×10^{-4}	6.2×10^{-6}
2×10^6	9.42×10^{-6}	308.6	3.610	2.18×10^{-4}	7.3×10^{-6}
3×10^6	1.23×10^{-5}	481.4	5.630	2.25×10^{-4}	7.1×10^{-6}
4×10^6	1.42×10^{-5}	664.0	7.700	2.30×10^{-4}	7.0×10^{-6}
5×10^6	1.57×10^{-5}	850.6	9.950	2.34×10^{-4}	6.8×10^{-6}
6×10^6	1.70×10^{-5}	1040	12.16	2.35×10^{-4}	6.8×10^{-6}

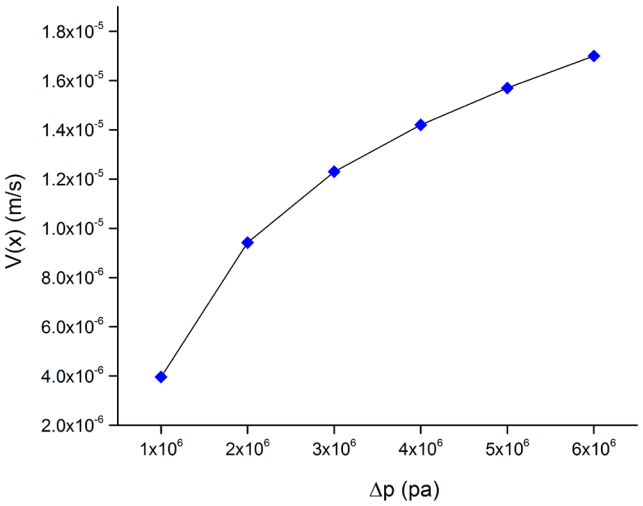

Fig. 2. Effect of applied pressure, Δ*p* on permeate velocity.

Table 3 displays the influence of changing bulk concentration on permeate velocity, wall concentration, concentration polarization factor and boundary layer thickness. Fig. 3 illustrates the relationship between water permeate velocity and feed concentration. It can be seen in Fig. 3 that permeate velocity decrease as feed concentration increases. An increase in feed concentration by 4% yield a decrease of 2.5% in permeate velocity. As given in the basic reverse osmosis equation [19], fouling is enhanced by the increase in the bulk concentration and consequently, the water permeate flux decreases.

Table 4 and Fig. 4 display the values of permeate velocity (*V(x)*) against the membrane water permeability. It is obvious in the figure that permeate velocity increases as membrane water permeability increases. Normally, water flux is directly proportional to the membrane water permeability as suggested by the basic reverse osmosis equations [6]. An increase in membrane water permeability by 17% yield an increase of 17% in permeate velocity. The effect of membrane water permeability on other factors such as wall concentration, concentration polarization factor, and boundary layer thickness is also depicted in Table 4.

3.2. Effect of operating parameters on wall concentration and concentration polarization factor

This subsection deals with the effect of operating parameters such as applied pressure, feed concentration and membrane water permeability on the wall concentration and concentration polarization factor. Fig. 5 exhibits a plot of wall concentration versus applied pressure. It is clear from the figure that the wall concentration increases with applied pressure, consequently concentration polarization increases. An increase in applied pressure by 17% yield an increase of 18% in wall concentration.

Fig. 6 depicts the effect of feed concentration on the membrane wall concentration. The wall concentration increases as the feed concentration increases as shown in the figure, where fouling is more pronounced. An increase in feed concentration by 4% yield an increase of 0.6 % in wall concentration.

Table 3
Effect of bulk concentration on water permeate velocity, wall concentration, concentration polarization factor and boundary layer thickness.

C_b, mol/m^3	$V_{(x)}$, m/s	C_w, mol/m^3	C_w/C_b	δ, m
75.50	9.96×10^{-6}	303.0	4.02	2.23×10^{-4}
80.50	9.68×10^{-6}	306.0	3.80	2.21×10^{-4}
85.50	9.42×10^{-6}	309.0	3.61	2.18×10^{-4}
90.50	9.17×10^{-6}	311.0	3.44	2.15×10^{-4}
95.50	8.93×10^{-6}	313.0	3.28	2.13×10^{-4}
100.5	8.70×10^{-6}	316.0	3.14	2.10×10^{-4}
105.5	8.49×10^{-6}	318.0	3.01	2.08×10^{-4}
110.5	8.27×10^{-6}	320.1	2.89	2.06×10^{-4}
115.5	8.07×10^{-6}	322.2	2.79	2.03×10^{-4}
120.5	7.87×10^{-6}	324.2	2.69	2.01×10^{-4}

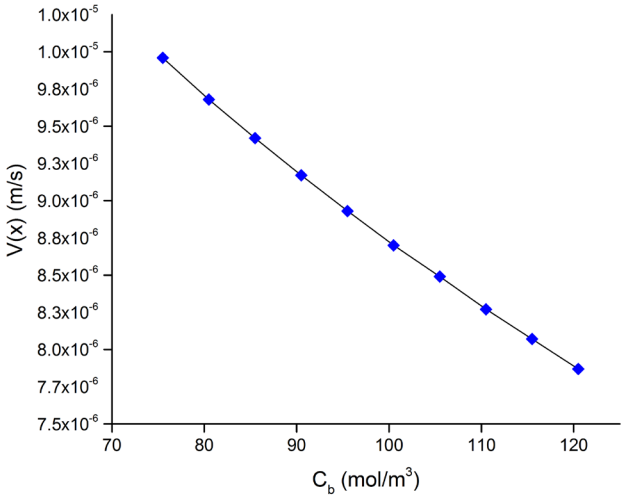

Fig. 3. Relationship between water permeate velocity and feed concentration.

Table 4
Impact of membrane water permeability on water permeate velocity, wall concentration, concentration polarization factor and thickness of boundary layer

A, m·pa^{-1}s^{-1}	$V_{(x)}$, m/s	C_w, mol/m^3	C_w/C_b	δ, m
1×10^{-11}	4.71×10^{-6}	308.6	3.609	4.36×10^{-4}
2×10^{-11}	9.42×10^{-6}	308.7	3.610	2.18×10^{-4}
3×10^{-11}	1.41×10^{-5}	308.7	3.610	1.45×10^{-4}
4×10^{-11}	1.88×10^{-5}	308.7	3.610	1.09×10^{-4}
5×10^{-11}	2.35×10^{-5}	308.8	3.611	8.72×10^{-5}
6×10^{-11}	2.83×10^{-5}	308.4	3.610	7.27×10^{-5}

Since both bulk concentration C_b and wall concentration C_w vary, therefore, the concentration polarization factor will depend on each value of bulk concentration and wall concentration as shown in Fig. 7. This can be explained by the variation of convective and diffusion effect. As bulk concen-

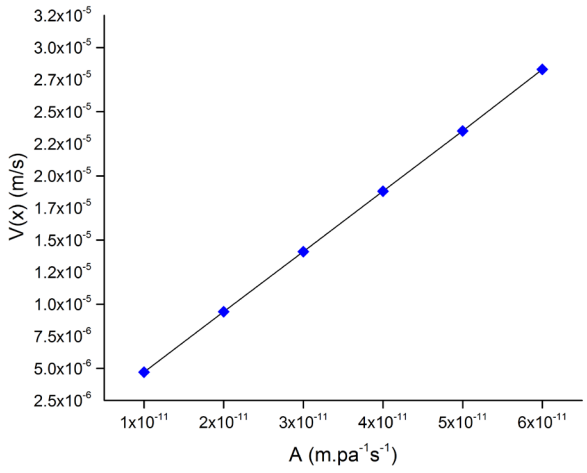

Fig. 4. Plot of water permeate velocity versus membrane water permeability.

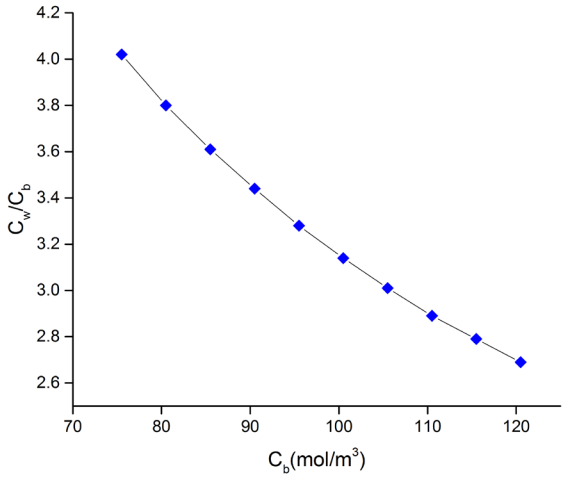

Fig. 7. Plot of concentration polarization factor vs. feed concentration.

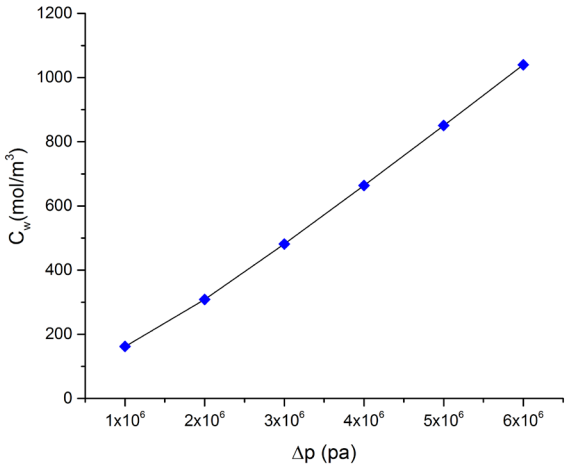

Fig. 5. Effect of applied pressure on the membrane wall concentration.

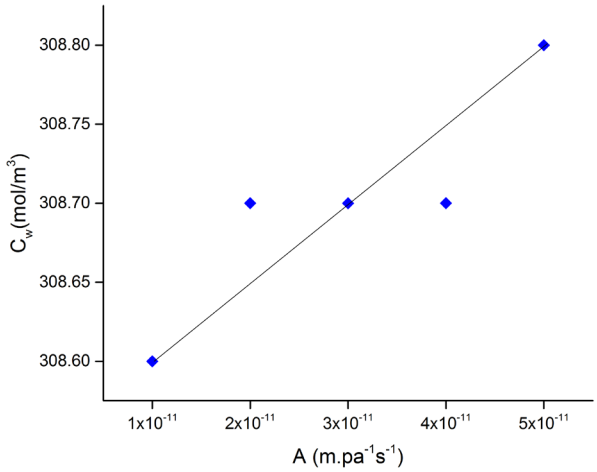

Fig. 8. Influence of membrane water permeability on wall concentration.

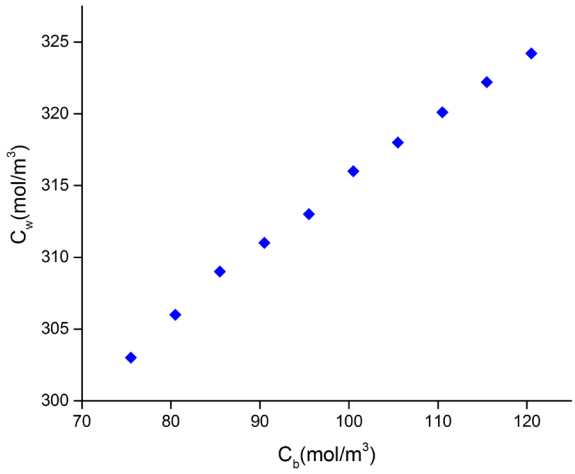

Fig. 6. Membrane wall concentration versus feed concentration.

tration increases, convective effect increases shrinking the boundary layer and reflect a slow increase in the wall concentration, so concentration polarization factor decreases as bulk concentration increases. An increase in feed concentration by 4% yield a decrease of 3.6% in concentration polarization factor.

Fig. 8 illustrates the effect of membrane water permeability on wall concentration. It is obvious from the figure that wall concentration increases as water permeability increases, that means an increase in concentration polarization. As membrane water permeability increases, more flux is produced yielding a small increase in wall concentration. An increase in membrane water permeability by 17% yield an increase of 0.13% in wall concentration.

3.3. Effect of operating parameters on boundary layer thickness

The effect of important operating parameters on boundary layer thickness is discussed in detail in this sec-

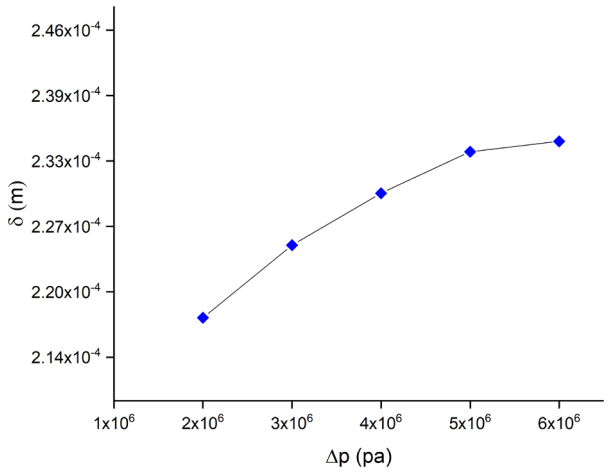

Fig. 9. Boundary layer thickness versus applied pressure.

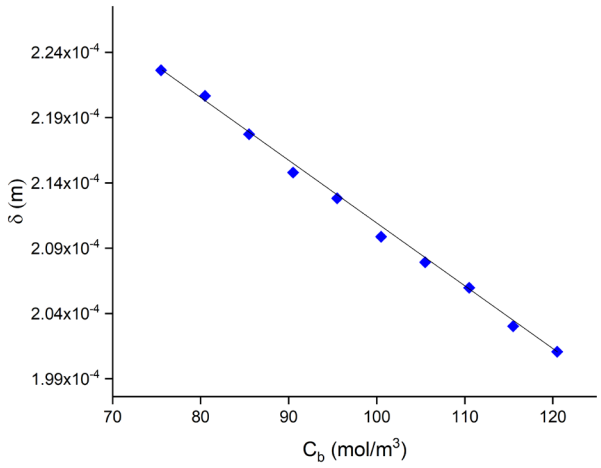

Fig. 10. Effect of feed concentration on boundary layer thickness.

tion. Table 2 displays the boundary layer thickness values against the applied pressure. Fig. 9 shows a plot of the boundary layer thickness and applied pressure. It can be observed from the figure that the boundary layer thickness is directly proportional to the applied pressure, however, it is not very clear in this figure. An increase in applied pressure by 17% yield an increase of 0.42% in boundary layer thickness.

Table 3 shows the boundary layer thickness values against the feed concentration. Fig. 10 displays a relationship between boundary layer thickness and feed concentration. It can be seen that the boundary layer thickness decreases as feed concentration increases which reflects an enlargement of the bulk region. An increase in feed concentration by 4% yield a decrease of 1% in boundary layer thickness.

Table 4 shows the boundary layer thickness (δ) values against the membrane water permeability. Fig. 11 demonstrates a plot of boundary layer thickness versus membrane water permeability. It is clear that boundary layer thickness decreases as membrane water permeability increases. An increase in membrane water permeability by 17% yield a decrease of 16.6 % in boundary layer thickness.

Upon reviewing the changes in boundary layer thickness with different operating parameters, it was found that the boundary layer thickness decreases with increase in both bulk concentration and membrane water permeability. But the increase of boundary layer thickness with increasing applied pressure is not very clear in Fig. 9. So, a plot of combined effect of applied pressure and bulk concentration was prepared as show in Fig. 12 and displayed in Table 5. The same observation was obtained, i.e. increase in the boundary layer thickness by increasing applied pressure.

Fig. 13 shows values of boundary layer thickness versus extended values of applied pressure. In Fig. 13, an expected decrease in the boundary layer thickness was observed with the increase in applied pressure for the lower values of applied pressure. This is due to a pronounce effect of convection, so boundary layer thickness decreases. When applied pressure increases, the wall concentration reach higher values and back diffusion is larger than the convection so the boundary layer thickness increases.

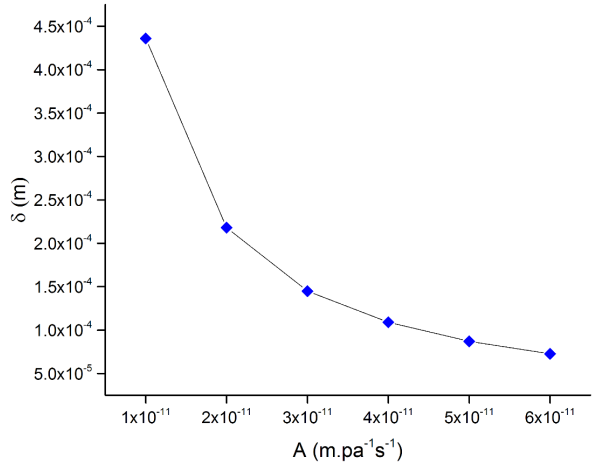

Fig. 11. Plot of boundary layer thickness vs. membrane water permeability.

Table 5
Study effect of changing both applied pressure and bulk concentration on boundary layer thickness

C_b	Δp	2.00×10^6	3.00×10^6	4.00×10^6
		δ (m)		
85.5		2.18×10^{-4}	2.25×10^{-4}	2.30×10^{-4}
90.5		2.01×10^{-4}	2.09×10^{-4}	2.15×10^{-4}
95.5		1.85×10^{-4}	1.95×10^{-4}	2.02×10^{-4}

4. Conclusions

In this work, a developed model describing concentration polarization in reverse osmosis process was used to perform the parametric analysis. Parametric study of concentration polarization was performed to investigate the effects of physical and operating parameters in point of view of the water permeate velocity, concentration polar-

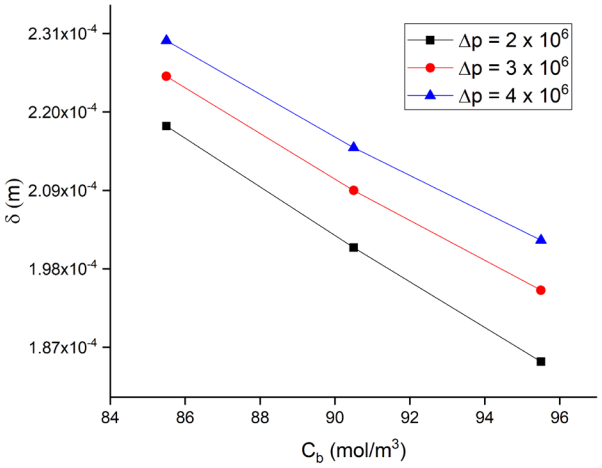

Fig. 12. Plot of boundary layer thickness versus bulk concentration at different applied pressures.

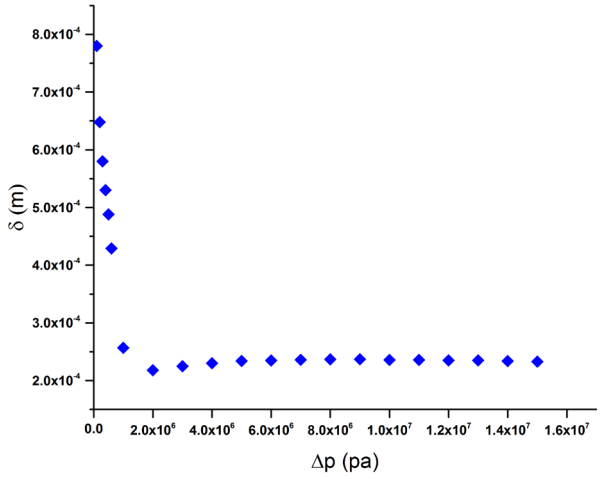

Fig. 13. Plot of applied pressure vs. boundary layer thickness.

ization, wall concentration and boundary layer thickness. The physical and operating parameters include; applied pressure, bulk concentration and membrane water permeability. It was found that the permeate water velocity increased with the increase in applied pressure and membrane water permeability while the feed concentration has reverse effect on the water permeate velocity. However, wall concentration was increased with the increase in all the physical and operating parameters (i.e. applied pressure, bulk concentration and membrane water permeability). The effect of different parameters on the boundary layer thickness was also studied and it was found that the boundary layer thickness decreases with increase in both membrane water permeability and feed concentration. But the increase of boundary layer thickness with increasing applied pressure was not very clear. Therefore,a plot of combined effect of applied pressure and bulk concentration was prepared. In this work, it is shown that by means of parametric analysis, the developed model will help researchers to obtain the optimum setting for reverse osmosis plants. A detailed parametric study was conducted to illustrate the variations of permeate velocity, wall concentration and membrane water permeability with different operating conditions such as applied pressure, feed concentration and boundary layer thickness. Hence, it can be concluded that the developed model is an efficient cost-effective tool to estimate the optimum parameters and evaluate the system performance of any reverse osmosis process.

Acknowledgment

The authors would like to extend their sincere appreciation to the Deanship of Scientific Research at King Saud University for its funding of this research through the Research Group Project number RGP-224.

Symbols

ϕ — Osmotic pressure coefficient, Pa/mol
γ — Wall shear rate, s^{-1}
ρ — Density of water, Kg/m^3
μ — Viscosity of water, $N{\cdot}s/m^{-2}$
Δp — Osmotic pressure, pa
Δp — Applied pressure, pa
A — Membrane water permeability, $m{\cdot}pa^{-1}\,s^{-1}$
C_b — Bulk concentration, mol/m^3
C_p — Product water concentration, mol/m^3
C_w — Membrane surface (wall) concentration, mol/m^3
d — Hydraulic diameter of channel, m
D — Diffusion coefficient, m^2/s
J_v — Product water flux across the membrane
K_b — Mass transfer coefficient, m/s
L — Channel length, m
R_o — Membrane salt rejection
R_m — Membrane resistance
R_e — Reynolds number
S_c — Schmidt number
S_h — Sherwood number
u — Water cross flow velocity, m/s

References

[1] I.S. Al-Mutaz, I. Wazeer, Comparative performance evaluation of conventional multi-effect evaporation desalination processes, Appl. Therm. Eng., 73 (2014) 1194–1203.
[2] I.S. Al-Mutaz, I. Wazeer, Optimization of location of thermo-compressor suction in MED-TVC desalination plants, Desal. Water Treat., 57 (2016) 26562–26576.
[3] I.S. Al-Mutaz, I. Wazeer, Development of a steady-state mathematical model for MEE-TVC desalination plants, Desalination, 351 (2014) 9–18.
[4] I.S. Al-Mutaz, I. Wazeer, Economic optimization of the number of effects for the multieffect desalination plant, Desal. Water Treat., 56 (2015) 2269–2275.
[5] I.S. Al-Mutaz, I. Wazeer, Current status and future directions of MED-TVC desalination technology, Desal. Water Treat., 55 (2015) 1–9.
[6] L. Henthorne, B. Boysen, State-of-the-art of reverse osmosis desalination pretreatment, Desalination, 356 (2015) 129–139.
[7] A. Malek, M. Hawlader, J. Ho, Design and economics of RO seawater desalination, Desalination, 105 (1996) 245–261.

[8] M. Elimelech, W.A. Phillip, The future of seawater desalination: energy, technology, and the environment, Science, 333 (2011) 712–717.
[9] L.F. Greenlee, D.F. Lawler, B.D. Freeman, B. Marrot, P. Moulin, Reverse osmosis desalination: water sources, technology, and today's challenges, Water Res., 43 (2009) 2317–2348.
[10] K.P. Lee, T.C. Arnot, D. Mattia, A review of reverse osmosis membrane materials for desalination—development to date and future potential, J. Membr. Sci., 370 (2011) 1–22.
[11] S. Kim, E.M. Hoek, Modeling concentration polarization in reverse osmosis processes, Desalination, 186 (2005) 111–128.
[12] M.G. Marcovecchio, P.A. Aguirre, N.J. Scenna, Global optimal design of reverse osmosis networks for seawater desalination: modeling and algorithm, Desalination, 184 (2005) 259–271.
[13] H.-J. Oh, T.-M. Hwang, S. Lee, A simplified simulation model of RO systems for seawater desalination, Desalination, 238 (2009) 128–139.
[14] J. Fernández-Sempere, F. Ruiz-Beviá, P. García-Algado, R. Salcedo-Díaz, Experimental study of concentration polarization in a crossflow reverse osmosis system using Digital Holographic Interferometry, Desalination, 257 (2010) 36–45.
[15] A.I. Radu, J.S. Vrouwenvelder, M. Van Loosdrecht, C. Picioreanu, Effect of flow velocity, substrate concentration and hydraulic cleaning on biofouling of reverse osmosis feed channels, Chem. Eng. J., 188 (2012) 30–39.
[16] W. Zhou, L. Song, T.K. Guan, A numerical study on concentration polarization and system performance of spiral wound RO membrane modules, J. Membr. Sci., 271 (2006) 38–46.
[17] A. Subramani, E.M. Hoek, Direct observation of initial microbial deposition onto reverse osmosis and nanofiltration membranes, J. Membr. Sci., 319 (2008) 111–125.
[18] D. Fletcher, D. Wiley, A computational fluids dynamics study of buoyancy effects in reverse osmosis, J. Membr. Sci., 245 (2004) 175–181.
[19] I.S. Al-Mutaz, F.M. Alsubaie, Development of a mathematical model for the prediction of concentration polarization in reverse osmosis desalination processes, Desal. Water Treat., 71 (2017) 19–24.
[20] G. Schock, A. Miquel, Mass transfer and pressure loss in spiral wound modules, Desalination, 64 (1987) 339–352.